Theory and Applications of Mathematics & Computer Science

(ISSN 2067-2764, EISSN 2247-6202)
http://www.uav.ro/applications/se/journal/index.php/tamcs

Theory and Applications of Mathematics & Computer Science 5 (2) (2015) 158– 185

Measure of Tessellation Quality of Voronoï Meshes

E. A-iyeh[a], J.F. Peters[a,b,*]

[a] *Computational Intelligence Laboratory, Department of Electrical & Computer Engineering, University of Manitoba, Winnipeg, MB, R3T 5V6, Canada.*
[b] *Department of Mathematics, Faculty of Arts and Sciences, Adıyaman University, Adıyaman, Turkey.*

Abstract

This article introduces a measure of the quality of Voronoï tessellations resulting from various mesh generators. Mathematical models of a number of mesh generators are given. A main result in this work is the identification of those mesh generators that produce the highest quality Voronoï tessellations. Examples illustrating the application of the quality measure are given in comparing Voronoï tessellations of digital images.

Keywords: Sites, Mesh Generation, Quality, Tessellations, Voronoï mesh.
2010 MSC: Primary 54E05, Secondary 20L05, 35B36.

1. Introduction

This article introduces a measure of the quality of Voronoï tessellations resulting from various mesh generators. A *Voronoï tessellation* is a collection of non-overlapping convex polygons called *Voronoï regions*. It is well-known that creating meshes is a fundamental and necessary step in several areas, including engineering, computing, geometric and scientific applications (Leibon & Letscher, 2000; Owen, 1998; Liu & Liu, 2004). Meshes assume simplex structures or volumes based on the geometry of the surfaces, dimension of the space and placement of sites of the meshes (see, *e.g.*, (Ebeida & Mitchell, 2012; Mitchell, 1993; Persson, 2004)). This work is a natural outgrowth of recent work on Voronoï tessellation (Persson, 2004; Persson & Strang, 2004; Bern & Plassmann, 1999; Du *et al.*, 1999; Brauwerman *et al.*, 1999; Peters, 2015*b*).

Seeds, generating points or sites of meshes for non-image domains may be chosen randomly, deterministically on grids (Persson, 2004), using distribution sampling *e.g.* (Ebeida & Mitchell, 2012), using the centroids of tessellation regions. In the search for a measure of mesh quality, it is

*Corresponding author: 75A Chancellor's Circle, EITC-E2-390, University of Manitoba, WPG, MB R3T 5V6, Canada; e-mail: james.peters3@ad.umanitoba.ca, research supported by Natural Sciences & Engineering Research Council of Canada (NSERC) discovery grant 185986.
Email addresses: umaiyeh@myumanitoba.ca (E. A-iyeh), James.Peters3@umanitoba.ca (J.F. Peters)

useful to identify the best or most suitable mesh generators (also called sites) for mesh generation. A principal benefit of this work is the identification of those generators that produce the highest quality Voronoï tessellations.

A natural application of the proposed mesh quality measure is given in comparing and classifying digital images Voronoï tessellation covers. Each Voronoï region is a closed set of points in a convex polygon. A Voronoï tessellation *cover* of a digital image equals the union of the Voronoï regions.

2. Related Work

Numerous mesh generation algorithms have been developed for several purposes including image processing and segmentation (Arbeláez & Cohen, 2006), clustering (Ramella *et al.*, 1998), data compression, quantization and territorial behavior of animals (Persson, 2004; Persson & Strang, 2004; Du *et al.*, 1999). These methods tackle a wide variety of geometrical representations for meshing the surfaces. In addition, a number of mesh generation algorithms are iterative in nature, so that the algorithm adjusts the meshes iteratively to approach fulfilling predefined conditions, thereby terminating on meeting the criterion up to some limits (Persson, 2004; Persson & Strang, 2004). In some adaptive mesh algorithms (Persson, 2004; Persson & Strang, 2004; George, 2006), the mesh sites are variable. For example they may be displaced to attain force equilibrium. In one such scenario the algorithm starts by partitioning the space based on the initial distribution of sites but iterates through them according to preset conditions on an element size function until the equilibrium and stopping conditions are satisfied (Persson, 2004). This essentially is refining and solving for optimality of the meshes (Rajan, 1994; Peraire *et al.*, 1987; Rivara, 1984; Ruppert, 1995) according to the preset conditions.

Voronoï diagrams introduced by the Ukrainian mathematician G. Voronoï (Voronoï, 1903, 1907, 1908) (elaborated in the context of proximity spaces in (Peters, 2015*b*), (Peters, 2015*c*), (Peters, 2015*a*)) provide a means of covering a space with a polygonal mesh. In telecommunications, Voronoï diagrams have furnished a tool of analysis for binary linear block codes (Agrell, 1996) governing regions of block code, performance of Gaussian channel among others. In music, Voronoï diagrams have once again demonstrated their utility (McLean, 2007). For example, they been successfully applied in automatic grouping of polyphony (Hamanaka & Hirata, 2002). Other works bordering on applications of Voronoï meshes in reservoir modeling (Møller & Skare, 2001), attempts at cancer diagnosis (Demir & Yener, 2005) are also available.

Ever since utility of Voronoï diagrams was demonstrated in several applications including the post office problem where given a set of post office sites in furnished the answer in determining the nearest one to visit and other few works of application of 56 meshed surfaces an area, Voronoï tessellation has been useful in the study of the territorial behavior of animals, image compression, segmentation etc no works or very few have focused on their application in proximity and classification analysis of digital images. This work proposes to explore the utility of meshes in the study of proximal regions as a means of image classification.

Mesh applications in image analysis are not widely studied in the open literature. In that regard, we seek to contribute to the application of meshes in image classification by (a) identifying the best forms of generating points for meshes, (b) arriving at a measure of the quality of meshes, and

(c) characterizing meshes best suited for image classification. In addition, it is anticipated that this research will yield useful theorems that are a natural outcome of measuring mesh quality. Such theorems provide a formal foundation for the study of image mesh quality.

3. Preliminaries

Since the discovery that Voronoï tessellations are the secret working formula of bees, humans have sought to bring similar benefits and applications of Voronoï tessellations in their applications to image processing, image compression, clustering, territorial behaviour of animals etc (Persson, 2004; Persson & Strang, 2004; Bern & Plassmann, 1999; Du *et al.*, 1999; Brauwerman *et al.*, 1999). Several forms of polygonal meshes exist due to Voronoï and Delaunay tessellations and since Delaunay triangulation is a dual of Voronoï, our focus will be on the former.

Assume a finite set S of locations called sites s_i in a space $\mathbb{R}^n$. Computing the Voronoï diagram of S means partitioning the space into Voronoï regions $V(s_i)$ in such a way that $V(s_i)$ contains all points of S that are closer to s_i than to any other object s_j, $i \neq j$ in S.

Given the generator set

$$S = \{s_1, , s_k : i \in \mathbb{N}\},$$

where each member of S is called a mesh generating point, let $s_i \in S$. The Voronoï region $V(s_i)$ is defined by

$$V(s_i) = \{x \in \mathbb{R}^n : \|x - s_i\| \leq \|x - s_k\|, s_k \in S, i \neq k\},$$

where $\|.,.\|$ is the Euclidean norm (distance between vectors). The set

$$V(S) = \bigcup_{s_i \in S} V(s_i)$$

is called the n-dimensional Voronoï diagram generated by the points in S. In $\mathbb{R}^2$, this effectively covers the plane with convex and non overlapping polygons, one for each generating point in S. A centroidal Voronoï tessellation is a special case of $V(s_i)$, where the sites are the mass centroids of regions computed by

$$c_i = \frac{\int_{V_i} x\rho(x)dx}{\int_{V_i} \rho(x)dx}$$

where $\rho(x)$ is the density function of $V(s_i)$. The mathematical utility of centroidal tessellations lie in their relationship to the energy function (Brauwerman *et al.*, 1999) defined as:

$$E(z, V) = \sum_{i=1}^{n} \int_{V_i} \rho(x)|x - z_i|^2 dx.$$

The energy function $E(z, V)$ for a Voronoï region depends on the density function $\rho(x)$ of the regions and the squared distances between the generating site z_i and nearby points x in the region. The total energy for a Voronoï diagram is the sum of integrals of the individual energies of the regions comprising the Voronoï diagram.

Voronoï regions are cells of growth from a certain view point. This view point is equivalent to considering the vertex of each region as a nucleus of a growing or expanding cell. Cells propagate

simultaneously outward from their nuclei at uniform rates until they intersect with others. They then freeze giving the boundaries of the regions defined by the tessellation.

Ultimately, cells whose nuclei are on the convex hull of a vertex grow until they intersect the outgrowth of others. It is interesting to note that since all cells are growing at the same rate, their first points of contact will coincide with the midpoint of the two nuclei. This is exactly the locus of all equidistant points from the nuclei.In other words it the perpendicular bisector of the the nuclei from which all points are equidistant. The set of all points on these loci form the edges of the regions.

Voronoï cells that share an edge are said to be Voronoï neighbors. The aggregate of triangles formed by connecting the nuclei of all Voronoï neighbors tessellate the area within the convex hull of the set. Notice that the regions obtained are neighborhoods defined by the norm $\|\cdot\|$. This makes it possible to have a continuous image-like treatment of a dot pattern, thus permitting the application of general image processing techniques (Ahuja & Schachter, 1982). One such interpretation of the Voronoï tessellation is to view it as a cluster partition of a space (Ramella *et al.*, 1998). In this view, the space is segmented by the various Voronoï regions, with the size of the clusters given by the areas of the regions. Also, the Voronoï tessellation is useful for boundary extraction, with the tessellated space viewed as a mosaic.

Definition 3.1. Given a point set $S \subseteq \mathbb{R}^n$ and a distance function d_n, the set $\{V_i\}_{i=1}^k$ is called a Voronoï tessellation of S if $V_i \cap V_j \neq \varnothing$ for $i \neq j$.

Definition 3.2. The Voronoï region of a site is a polygon about that site. The set of all regions partition the plane of the sites S based on a distance function $\|\cdot\|$. This results in the plane being covered with polygons about those sites.

Definition 3.3. Given a set $S = \{s_1, ..., s_k\}$ of points, any plane (v_i, v_j) is a Voronoï edge of the Voronoï region V if and only if there exists a point x such that the circle centered at x and circumscribing v_i and v_j does not contain in its interior any other point of V.

Definition 3.4. A Voronoï tessellation is a set of polygons with their edges and vertices that partition a given space of sites.

Definition 3.5. A Voronoï edge is a half plane equidistant from two sites and which bounds some part of a Voronoï region. Every edge is incident upon exactly two vertices and every vertex upon at least three edges.

Definition 3.6. A Voronoï vertex is the center of a circle through three sites.

Definition 3.7. A set of points form a convex set if there is a line connecting each pair of points.

Definition 3.8. The convex hull of Voronoï regions about a set of sites is the smallest set which contains the Voronoï regions as well as the union of the regions.

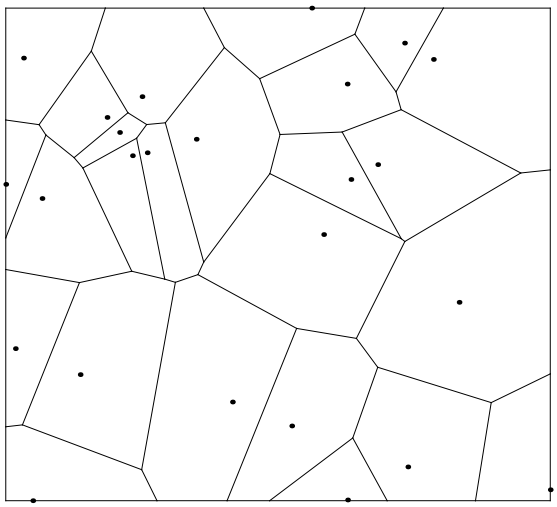

Figure 1. Voronoï diagram of a set of sites.

Definition 3.9. A dot or point pattern is a set of points of a signal representing spatial locations of signal features. For example sets of corners, keypoints etc are referred to as point or dot patterns.

Definition 3.10. The quality of a signal is defined as a characteristic of the signal which gives information about perceived signal degradation compared to an ideal.

Lemma 3.1. *The energy of a point located in a particular Voronoï region $V(s_i)$ is minimal with respect to all other regions $V(s_j)$ for $i \neq j$.*

Proof. Consider a point $y \in V(S_i)$. Its energy is evaluated as:

$$E(z, V) = \int_{V_i} \rho(y)|y - \hat{z}_i|^2 dy$$

$$E(z, V) = \int_{V_i} \rho(y)(0)dy = 0.$$

Since the distance between z and y is 0 by definition, $E = 0$. However E(z,V) of $y \notin V(S_j)$ is

$$E(z, V) = \int_{V_j} \rho(y)|y - \hat{z}_i|^2 dy \neq 0.$$

Since $\rho(y)$ nor $|y - \hat{z}_i|^2$ is non-zero. □

Theorem 3.1. *The energy function $E(z, V)$ is minimized at the centroid sites of the tessellations.*

Proof.

$$E(z, V) = \sum_{i=1}^{n} \int_{V_i} \rho(x)|x - \hat{z}_i|^2 dx.$$

The energy of a Voronoï region V_i is the integral of the product of the density function of that region $\rho(x)$ and the squared distances between the generating site $\hat{z}_i$ and points comprising the region. The total energy $E(z, V)$ is the sum of the energies of all Voronoï regions.

To obtain the minimum of $E(z, V)$, it requires that the derivative of the function with respect to the sites be equal to zero. The solution of the derivative are the sites $\hat{z}_i$.

$$\frac{dE}{d\hat{z}_i} = 2\sum_{i=1}^{n}\int_{V_i}\rho(x)(x-\hat{z}_i)dx = 0$$

$$\hat{z}_i = \frac{\int_{V_i} x\rho(x)dx}{\int_{V_i}\rho(x)dx}.$$

The solution $\hat{z}_i$ are the centroids. □

Theorem 3.2. *For a given set of sites $Z = \{z_i\}$, the energy is minimized when V is a centroidal Voronoï tessellation.*

Proof. Immediate from Lemma 3.1 and Theorem 3.1. □

4. Tessellation Generators

In the literature few works or none considers the choice of sites for meshing images using location of image features. We mostly go ahead and tessellate using chosen locations irrespective of locations of image features. Previously, sites have been chosen to correspond to center of masses of regions (Du *et al.*, 1999; Burns, 2009), random locations (Ebeida *et al.*, 2011; Aurenhammer, 1991), deterministic or regular locations (Persson, 2004; Persson & Strang, 2004; Aurenhammer, 1991). In short, majority of these locations do not take information of the sites into account. The method of centroids has evident advantages (Brauwerman *et al.*, 1999), but these are questionable if the regions from which we obtain the center of masses do not reflect image feature locations. In this work, various sites based on image features are first discovered and subsequently the sites give a tessellation of the space. With several sites found and tessellations performed, quality measures of the meshes are obtained with the view of helping ascertain the best sites for tessellations using an overall quality measure. This then forms a road map to meshed image analysis given a method of sites that yield high quality meshes. Important image features are known to reside at corner, edge, keypoints, centroids, extrema and modal image feature sites. These then would be used to discover mesh sites. They are treated next.

4.1. Image Corner Points

A very notable feature of digital images are image corner points. These define points where structures in the image intersect, as such they form a solid background for feature recognition and extraction.

One of the earliest criteria for corner point identification is a point that has low self-similarity (Moravec, 1980). Each pixel centered in a patch is compared to nearby pixels in an overlapping patch for corner point candidate examination. Since then, improvements in corner point identification by computing differential corner scores with respect to direction instead of patches in

(Moravec, 1980) resulted in combined corner and edge detection (Harris & Stephens, 1988). For more accuracy in subpixels in corner identification see (Förstner & Gülch, 1987). Recently, corner detection based on other methods: Multiple scales due originally to (Harris & Stephens, 1988), level curvature approach (Kitchen & Rosenfeld, 1980; Koenderink & Richards, 1988), difference of Laplacians, Gaussians, and Hessians (Lowe, 2004; Lindeberg, 1998, 2008), affine-adapted interest point operators (Lindeberg, 1993, 2008; Mikolajczyk & Schmid, 2004), curvature placement along edges (Wang & Brady, 1995), smallest univalue segment assimilating nucleus (Smith & Brady, 1997), direct testing of pixel self-similarity and feature accelerated segment (Rosten & Drummond, 2006), non-parametric and adaptive region processing methods (Guru & Dinesh, 2004), transform approaches (Kang *et al.*, 2005; Park *et al.*, 2004), adaptive approaches (Pan *et al.*, 2014), structure-based analysis (Kim *et al.*, 2012) have resulted . Corner points are identified here as points in which there is a significant change in intensity features in two or more directions:

$$C(u,v) = \sum w(x,y)[I(x+u,y+v) - I(x,y)]^2.$$

The window function $w(x,y)$ tends to be rectangular but could assume other suitable forms. So, a corner point is returned by the corner point function $C(x,y)$ if the squared intensity difference between the intensity at location (x,y) and location $(x+u,y+v)$ is large for any two directions.

4.2. Edge Sites

Edge maps are widely used in image processing for feature detection and object recognition. Besides, edge information is known to be crucial in feature detection and image analysis. These have been used due to the fact that the edges tend to localize an object of interest for target processing and feature detection. Edge points are points whose feature values differ sharply from those of neighboring points (Canny, 1986).

4.3. Image Keypoint Sites

Image keypoints are popular for extracting distinct image points (Lowe, 1999; Mitchell, 2010; Feng *et al.*, 2013; Woźniak & Marszałek, 2014). Scale-space extrema detection has been shown to yield image keypoints (Lowe, 1999). This process however usually yields numerous keypoint candidates therefore we have to resort to means of reducing their number to important ones. For example by eliminating low contrast points, the most important ones are retained. Detection of locations of keypoints invariant to scale change may be accomplished by obtaining stable features across scales of an image (Lowe, 1999). In that regard, the scale space $L(x,y,\sigma)$ is obtained by convolution of Gaussian functions $G(x,y,\sigma)$ with the image function $I(x,y)$ at several scales k.

$$L(x,y,\sigma) = G(x,y,\sigma) * I(x,y)$$

$$G(\vec{x},\sigma) = \frac{1}{2\pi\sqrt{\sigma}}\mathrm{Exp}\{-\frac{1}{2}(\vec{x}-\mu)^T\sigma^{-1}(\vec{x}-\mu)\}.$$

We proceed below to obtain the difference of the convolved result in the previous step.

$$D(x,y,\sigma) = (G(x,y,k\sigma) - G(x,y,\sigma)) * I(x,y)$$

$$D(x, y, \sigma) = L(x, y, k\sigma) - L(x, y, \sigma).$$

In the final step, the extrema (minima and maxima) points are obtained by comparing points in the difference functions and selecting those that achieve the minimum or maximum values in their neighborhoods (Lowe, 1999). Keypoint locations originally found at $D(x, y)$ at scales of σ may be used as estimates in Taylor series expansion about the position vector $\vec{x} = (x, y)$ to obtain more accurate locations of the points (Brown & Lowe, 2002). Locations are extrapolated as follows.

$$D_a(\bar{x}) = D + \frac{\partial D^T}{\partial \vec{x}} + \frac{1}{2}\vec{x}\vec{x}^T \frac{\partial^2 D}{\partial \vec{x}^2 \vec{x}},$$

where $D_a(\bar{x})$ is the improved location of a keypoint.

4.4. Centroid Sites

Given a tessellated plane of points centroid points of regions are computed as follows.

$$c_i = \frac{\int_{V_i} x\rho(x)dx}{\int_{V_i} \rho(x)dx}.$$

The center of masses c_is are computed from Voronoï regions and then used to re-tessellate the regions. Given corner, edge and keypoint sites in images, their tessellations produce Voronoï regions corresponding to those generators. The centers of masses of these regions based on those image feature locations form a set of sites in the plane for centroidal tessellations.

4.5. Modal Pixel and Extrema Sites

The histogram distributions of images are readily available. They furnish information on the distribution of the pixels in the image. Pivotal points in an image can be sought by considering the modal pixel positions in the image. In this way, we get to find out the feature value that occurs most frequently in a digital image and use the locations of those as sites for tessellations. A variant to this approach is to find the modal feature value, displace it by a constant and then use the positions of the resulting value as sites for image tessellations. The most influential feature M is obtained from the histogram distribution $h(k)$ from the steps below.

$$h(k) = \sum_x \sum_y n_k$$

$$M = \mathrm{Max}_k(\sum_x \sum_y n_k) = \mathrm{Max}_k(hk).$$

For a given image function $I(x, y)$, the feature values are in the range $[0, k]$. From this set, there exists minimum and maximum feature values. Sites corresponding to the extrema can be used for tessellations. However, it should be noted that where any of the extrema is unique, only one site is returned for the tessellation. Extrema sites M_1, M_2, M_d are useful because they can give us geometrical information about objects that tend to have a particular distribution or feature value;

$$M_1 = \mathrm{Min}(f(x, y) \forall x, y)$$

$$M_2 = \text{Max}(f(x,y) \forall x,y)$$
$$M_d = \text{Max}(\sum\sum n_{ij}) - a.$$

Extrema sites are discovered using M_1 and M_2, whilst displaced modal sites are discovered using M_d, given the constant a. Due to the numbers of modal and extrema sites and the nature of meshes they produce, they are not treated further in this work. Instead, displaced feature sites are discovered and used.

So far, we have identified sites of important features in digital images. A necessary step in determining the choice of sites lies in the quality of meshes produced by the particular choice of sites. In what follows, the quality of meshes produced by the sites is examined.

5. Voronoï Mesh Quality Analysis

Quality metrics for mesh analysis have been explored in the literature (Knupp, 2001; Shewchuk, 2002; Bhatia & Lawrence, 1990*a*). Most mesh generation approaches set a predefined quality factor for each cell as such they easily achieve meshes with high quality. This is not always useful or justifiable. For example, in images it's highly unlikely that mesh sites are deterministically or randomly distributed as assumed in these methods, thus this work discovers sites using image features with the view point of obtaining quality factors as high as possible.

Let X be a nonempty set of polygons in a Dirichlet tessellation, $x, y \in X$. A polygon $x \in X$ in a tessellation is called a **cell**. A question that arises naturally is that which sites are best or more favorable, leading to high quality cells? We will attempt to answer this in terms of the overall mesh quality factor q_{all} for the mesh cells produced by a particular set of sites. Qualities of individual mesh cells computed here are defined according to the geometry of the cell (Shewchuk, 2002; Bhatia & Lawrence, 1990*a*).

Let S be a set of tessellation cells, A the area of a tessellation containing a 3-sided polygon cell $s \in S$, l_1, l_2, l_3 the lengths of the sides of s with $Q(s)$ the quality of cell s. Then, for example, (Bhatia & Lawrence, 1990*b*), (Bank & Xu, 1996) as well as (Field, 2000) use the following smooth quality measure for a 3-sided cell.

$$Q_3(s) = 4\sqrt{3}\frac{A}{l_1^2 + l_2^2 +, l_3^2}.$$

For a four sided mesh cell, the quality factor $Q_4(s)$ is defined by

$$Q_4(s) = \frac{4A}{l_1^2 + l_2^2 + l_3^2 + l_4^2}.$$

The quality $Q(s)$ of $3D$ tetrahedron (polyhedron with 4 sides) cell in $\mathbb{R}^3$ is defined by

$$Q_{43D}(s) = \frac{6\sqrt{2}V}{l_{rms}^3}.$$

Here, V is the volume of the tetrahedron and l_{rms} is given by:

$$l_{rms} = \sqrt{\frac{1}{6}\sum_{i=1}^{6} l_i^2}.$$

Since the focus is on meshes of $2D$ surfaces in $\mathbb{R}^2$, we only briefly consider $3D$ meshes. An overall mesh quality indicator may be defined for any meshed surface by making use of the qualities of the individual cells. One such indicator is defined by q_{all} defined below.

$$q_{all} = \frac{1}{N}\sum_{i=1}^{N} q_i.$$

For a plane tessellated by a set of sites S, the indicator of the overall tessellation quality is influenced by the qualities of the individual cells q_i. This provides a useful tool for discriminating sites and their tessellation quality.

Theorem 5.1. *For any plane, there exists a set of sites for which the mesh quality is maximum.*

Proof. Consider an arbitrary n-sided mesh cell. Assume the cell is a quad cell without loss of generality. For maximum q, the partial derivatives of q with respect to the l_is should be equal.

$$\frac{\partial q}{\partial l_1} = \frac{\partial q}{\partial l_2} = ... = \frac{\partial q}{\partial l_n}$$

$$\frac{-8Al_1}{(l_1^2 + l_2^2 + ... + l_n^2)^2} = \frac{-8Al_2}{(l_1^2 + l_2^2 + ... + l_n^2)^2} ... = \frac{-8Al_n}{(l_1^2 + l_2^2 + ... + l_n^2)^2}.$$

This happens when $l_1 = l_2 = ... = l_n$. So generators chosen such that their half planes are equidistant from each other would satisfy this condition. □

To synthesize and crystallize the preceding deliberations on mesh quality analysis, the following algorithm is provided.

5.1. Algorithm for Mesh Quality Computation

It is clear that a Voronoï diagram is a collection of several polygons of different dimensions in accordance with the criteria already laid out, thus the quality factor of each polygon is computed as follows:

Input: set of sites S, set of cells $V(S)$
Output: Mesh Quality(Q(s))
for each Voronoï region $V_i(s) \in V(S)$, site $s \in S$ **do**
  Access the number of sides and coordinates of the vertices of the polygon;
  Using the coordinates, compute the lengths l_i and Area A of the polygon;
  Use l_i and A in the appropriate expression to compute cell quality $Q(s)$, $s \in S$;
end for
$Q(S) = \{Q(s)\}$ ■

The results presented in the following sections show tessellated image spaces side-by-side with the distribution of the quality factors of their cells. These are shown for image data of several subjects. From the distribution of quality factors, we obtain the mean quality measure as an indicator of overall quality of meshes due to each set of generating sites.

6. Application: Digital Image Tessellation Quality

Mesh sites are obtained using the $2D$ face sets from (Craw, 2009). The images are monochrome with dimensions 181 by 241 showing subjects with different expressions and orientations. The sites so obtained from them are used to tessellate the regions and subsequently, quality factors of cells are computed. The quality factors are shown in histogram plots next to the tessellated images (Fig. 2-Fig. 21).

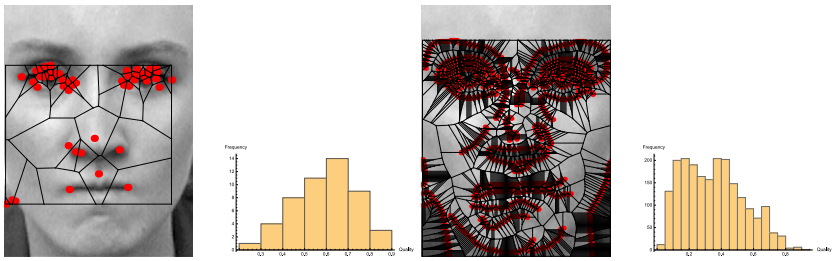

2.1: Corners 2.2: CorHist 2.3: Edges 2.4: EdHist

Figure 2. Corner & Edge Tessellations and Quality Histograms.

Remark 6.1. Corner-Based vs. Edge-Based Voronoï Tessellations.
A corner-based Voronoï tessellation of a face image is shown in Fig. 2.1. The corresponding corner-quality mesh histogram is given in Fig. 2.2. The horizontal axis represents mesh cell qualities and vertical axis represents the frequencies of the qualities. Because the number of image corners found are both sparse and grouped together in the facial high points representing pixel gradient changes in directions, the corresponding corner-based mesh consists of fairly large polygons surrounding the corners. Also, observe that the corner-based mesh histogram has a fairly normal distribution (skewed to the right).

An edge-based Voronoï tessellation of a face image is shown in Fig. 2.3. The corresponding edge-quality mesh histogram is given in Fig. 2.4. By contrast with image corners used as mesh generating points, the number of edge pixels found is large. In addition, the edge pixels are grouped closely together. Hence, the corresponding edge-based mesh contains many small Voronoï regions grouped closely together. The resulting edge-based mesh histogram has more than one maximum, which is an indicator that edge-based meshes have poor quality. □

Remark 6.2. Dominant-Based vs. Keypoint-Based Voronoï Tessellations.
Fig. 3.1 shows dominant-based tessellations alongside their quality measures in Fig. 3.2. Similarly, keypoint-based tessellations and their qualities are shown in Fig. 3.3 and Fig. 3.4 respectively. Dominant-based cells tend to have quality values that fall within several ranges of the quality scale. Even though dominant generators tend to have higher numbers like edge generators, they generally give higher qualities compared to edge-based cells. Keypoint-based cells like dominant-based cells tend to have their qualities falling in several ranges of quality, only that the number of fragmented ranges is usually smaller compared to that of dominant-based cells. Even

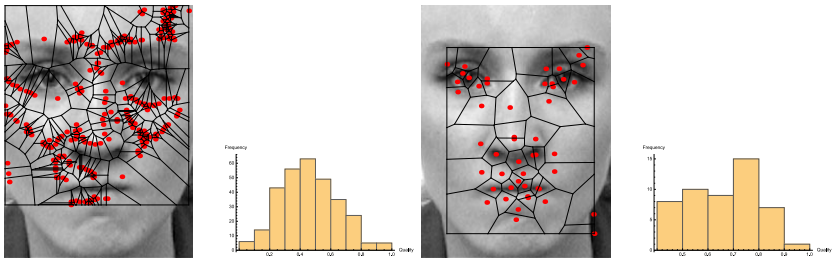

3.1: Dominants 3.2: DomHist 3.3: Keypts 3.4: KeyHist

Figure 3. Dominant & Keypoint Tessellations and Quality Histograms.

though keypoint generators have smaller numbers compared to dominant generators, the location and distribution of the features favor creation of more perfect mesh cells. The qualities of dominant-based cells peak around mid scale whilst those of keypoints tend to be flat. □

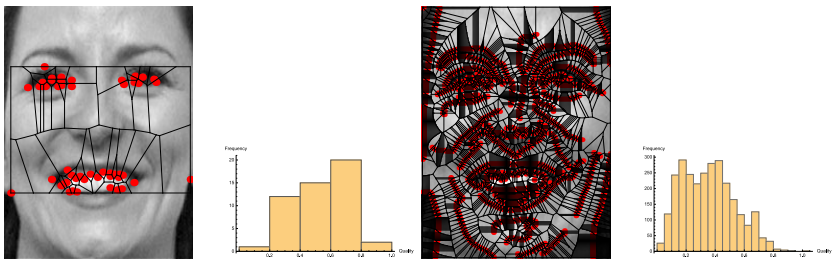

4.1: Corners 4.2: CorHist 4.3: Edges 4.4: EdHist

Figure 4. Corner & Edge Tessellations and Quality Histograms.

Remark 6.3. Corner-Based vs. Edge-Based Voronoï Tessellations.
The corner generators of Fig. 4.1 are concentrated in the mouth and eye regions of the subject. As a consequence, unequal distribution of the cell qualities in those regions result in Fig. 4.2. Edge-based cells on the other hand are distributed around the borders of the entire image giving peak cell quality in about mid range of the scale (see Fig. 4.3, Fig. 4.4). □

Remark 6.4. Dominant-Based vs. Keypoint-Based Voronoï Tessellations.
Dominant generators outweigh keypoints in number (see Fig. 5.1,Fig. 5.3). The generators are however concentrated around the mouth and eye regions but with extra points around the chin region in the case of dominant generators. Due to these distributions of the generators, both sets of generators have comparatively high qualities with peculiar quality factor distributions as shown in Fig. 5.2 and Fig. 5.4. □

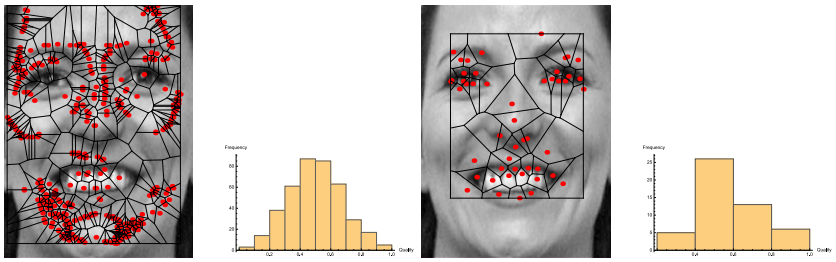

5.1: Dominants 5.2: DomHist 5.3: Keypts 5.4: KeyptHist

Figure 5. Dominant & Keypoint Tessellations and Quality Histograms.

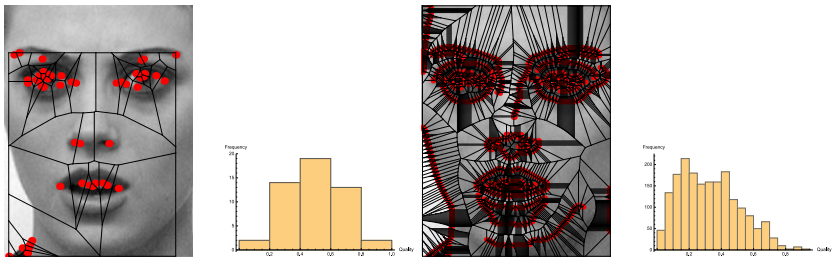

6.1: Corners 6.2: CorHist 6.3: Edges 6.4: EdHist

Figure 6. Corner & Edge Tessellations and Quality Histograms.

Remark 6.5. Corner-Based vs. Edge-Based Voronoï Tessellations.
Sets of generators of a subject are shown in Fig. 6.1 and Fig. 6.3. In addition to generators around the eye and mouth regions, generators around the nose and lower neck areas are returned for corner sites. Edges on the other hand are returned for regions of feature discontinuities. The quality plots of Fig. 6.2 and Fig. 6.4 represent the cells with more well laid out features on one hand and clustered generators on the other. □

Remark 6.6. Dominant-Based vs. Keypoint-Based Voronoï Tessellations.
Dominant generators returned here exclude most of the keypoint generators (Fig. 7.1,Fig. 7.3). Also, keypoint generators are more localized as opposed to the more or less global distribution of dominant generators. These fundamentally different generators produced a somewhat flat distribution of cell qualities (taken in two halves) and an alternating distribution of qualities seen in Fig. 7.4 and Fig. 7.2 respectively. □

Remark 6.7. Corner-Based vs. Edge-Based Voronoï Tessellations.
Distinct generators are returned in the case of Fig. 8.1 as opposed to less distinct ones in Fig. 8.3. Although corner generators are smaller in number, they have covered a lot of distinct and important features in the image. Edge generators however are localized to boundary regions. Given the layout of generators, the corner generators favored creating meshes approaching perfect lengths than edge generators as seen in Fig. 8.2 and Fig. 8.4 respectively. □

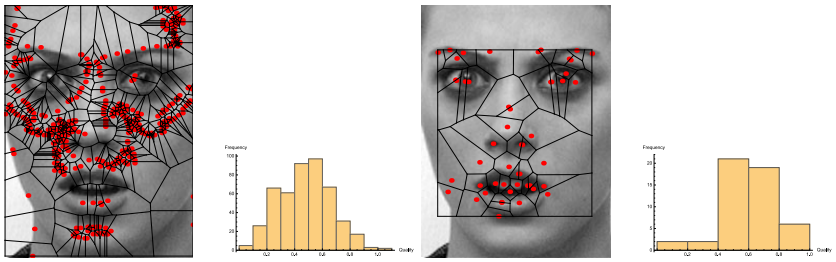

7.1: Dominants 7.2: DomHist 7.3: Keypts 7.4: KeyptHist

Figure 7. Dominant & Keypoint Tessellations and Quality Histograms.

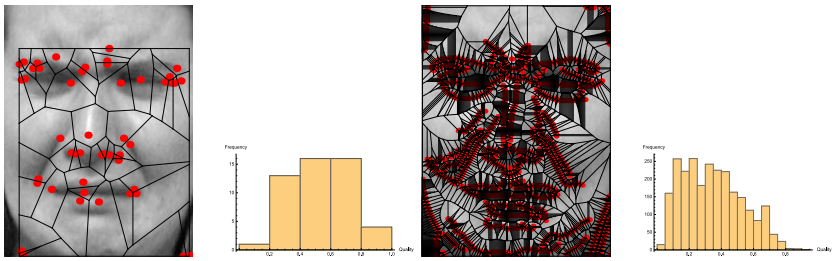

8.1: Corners 8.2: CorHist 8.3: Edges 8.4: EdHist

Figure 8. Corner & Edge Tessellations and Quality Histograms.

Remark 6.8. Dominant-Based vs. Keypoint-Based Voronoï Tessellations.
In Fig. 9.1 the layout of the generators does not favour polygons with equal lengths. This is evident in the fragmented nature of the quality factors in Fig. 9.2. Generators however in Fig. 9.3 performed better in their quality distributions in Fig. 9.4. □

Remark 6.9. Corner-Based vs. Edge-Based Voronoï Tessellations.
Examine for a brief moment the corner and edge generators in Fig. 10.1 and Fig. 10.3 alongside their quality factors in Fig. 10.2 and Fig. 10.4 respectively. Notice that some generators are clustered around the eye regions. The situation however is still better in terms of affording better overall quality as opposed to similar clustering of edge detectors in several areas. □

Remark 6.10. Dominant-Based vs. Keypoint-Based Voronoï Tessellations.
Dominants and their tessellations in Fig. 11.1 occupy a larger area compared to keypoints and their tessellations in Fig. 11.3. Although many cells result in Fig. 11.2, most of the quality factors are concentrated in the first half of the scale. Keypoints on the other hand are better laid out and although of a smaller number, they cover a comparable space and give a higher overall quality measure from Fig. 11.4. □

A complete set of results based on centroids of Voronoï regions specified by corner, edge, dominant and keypoint tessellations is shown in Fig. 12-Fig. 21. For those results shown, generators have been obtained corresponding to Voronoï regions of corner, edge, dominant and keypoint

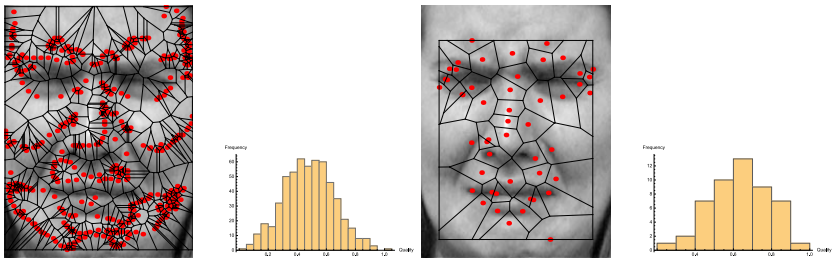

9.1: Dominants 9.2: DomHist 9.3: Keypts 9.4: KeyptHist

Figure 9. Dominant & Keypoint Tessellations and Quality Histograms.

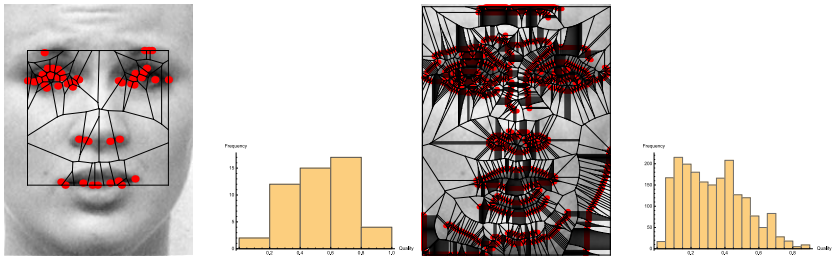

10.1: Corners 10.2: CorHist 10.3: Edges 10.4: EdHist

Figure 10. Corner & Edge Tessellations and Quality Histograms.

tessellations. These are the centroids of Voronoï regions in Fig. 2-Fig. 11. In the following text, remarks are included pertaining to the regions and their qualities.

Remark 6.11. Corner centroid-Based vs. Edge centroid-Based Voronoï Tessellations.
In comparing Fig. 2.1 to Fig. 12.1 we notice that the numbers of generators is the same. However, an interesting situation arises. The polygons in the latter case have a reduced variability in their lengths. This led to better quality measures with quality distributions as in Fig. 12.2. In a similar vein the number of generators are the same for edge generators and edge-centroid generators. The overall quality has been improved from the neighborhoods of 0.3 to above 0.5 (Fig. 12.3,Fig. 12.4). □

Remark 6.12. Dominant centroid-Based vs.Keypoint-Based Voronoï tessellations.
Notice that the locations of centroid generators are different from those of dominant generators. This distribution led to a mesh covering of about three quarters of the image as seen in Fig. 13.1. These generators favored better mesh qualities with the distribution seen in Fig. 13.2. Keypoint centroids of Fig. 13.3 and their tessellations however cover comparable areas with keypoint generators. The use of the centroid generators improved the mesh qualities as shown in Fig. 13.4. □

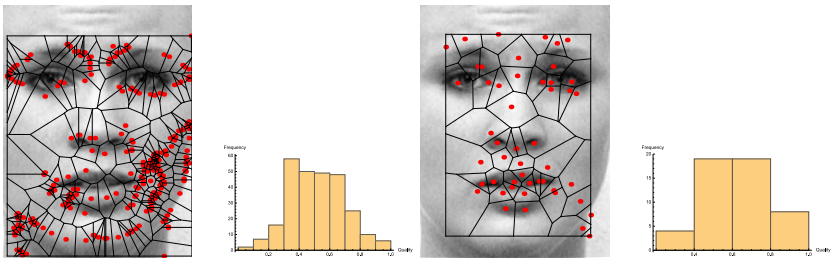

11.1: Dominants 11.2: DomHist 11.3: Keypoints 11.4: KeyptHist

Figure 11. Dominant & Keypoint Tessellations and Quality Histograms.

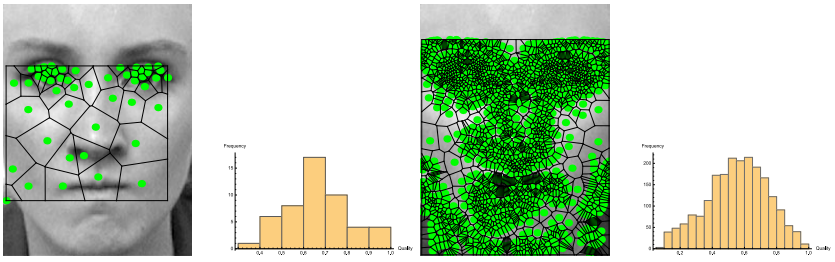

12.1: Corner-centroids 12.2: CornerCentHist 12.3: Edcentroids 12.4: EdcentHist

Figure 12. Corner & Edge Centroid Tessellations and Quality Histograms.

Remark 6.13. Corner centroid-Based vs.Edge centroid-Based Voronoï Tessellations.
The centroid sites of Fig. 14.1 barely covered the eyes, nose and most of the mouth region. As expected, edge centroids cover and tessellate the entire image Fig. 14.3. Although the mesh qualities are improved, they are consistent with distribution of cell lengths in Fig. 14.2 and Fig. 14.3. □

Remark 6.14. Dominant centroid-Based vs.Keypoint-Based Voronoï tessellations.
Observe in the tessellated spaces that the dominant centroid generators are mostly clustered in all areas except in the eyes and the mouth (see Fig. 15.1). Keypoint centroids however are distributed primarily around the facial features such as the mouth, nose and mouth as observed in Fig. 15.3. These generators are less clustered compared to their counterparts for dominant and keypoint generator tessellations. With the favorable condition for improved cell qualities obtained by using the centroids, the qualities are distributed across the entire quality scale as seen in Fig. 15.2 and Fig. 15.4. In most of the cases, the minimum cell quality for keypoint centroid-based generators is in the neighborhoods of 0.4-0.5. □

Remark 6.15. Corner centroid-Based vs.Edge centroid-Based Voronoï Tessellations.
Observe that several generators are located in the eye ball regions in Fig. 16.1. The tessellated regions cover up to the chin region. Less varying polygonal lengths led to distribution of mesh

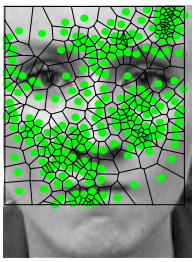

13.1: Dominant-centroids

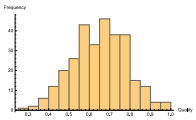

13.2: DomcentHist

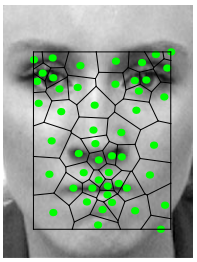

13.3: Keyptcentroids

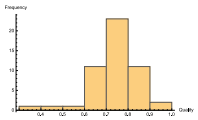

13.4: KeyptcentHist

Figure 13. Dominant & Keypoint Centroid Tessellations and Quality Histograms.

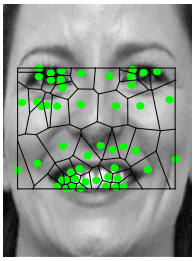

14.1: Corcentroids

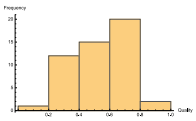

14.2: CorcentHist

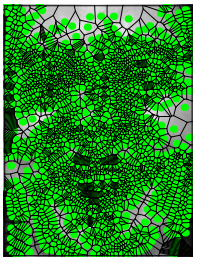

14.3: Edgecentroids

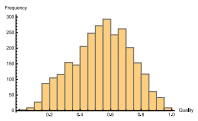

14.4: EdcentHist

Figure 14. Corner & Edge Centroid Tessellations and Quality Histograms.

qualities in Fig. 16.2. Most of the image plane is however covered by edge centroid generators (Fig. 16.3). Although the quality factors are fragmented, they cover the entire scale with the distribution shown in Fig. 16.4 with minimum quality starting at about 0.3. □

Remark 6.16. Dominant centroid-Based vs.Keypoint-Based Voronoï tessellations.
Dominant generators cover most of the image plane. However, most of the generators tend to be concentrated just below the eyes and nose regions. Also notice that regions without clustering of the cells tend to be polygons whose lengths tend to be equal. This distribution of the generators affords cells and qualities in Fig. 17.1 and Fig. 17.2. Although there are keypoint centroid generators in the eye, nose and mouth regions, they are not clustered as in the previous case (see Fig. 17.3). They are better spaced out giving the qualities in Fig. 17.4. □

Remark 6.17. Corner centroid-Based vs.Edge centroid-Based Voronoï Tessellations.
Centroid corner generators tessellate the image region around the facial features. This placement of the generators yielded cells with flat distribution of qualities across the scale (see Fig. 18.1, Fig. 18.2). Edge centroid generators on the other hand tessellated the entire image but with the sites clustered together in most areas. Even though the whole image space is covered, the resulting cells do not promote better overall quality as compared with centroidal corner tessellations (see Fig. 18.3, Fig. 18.4). □

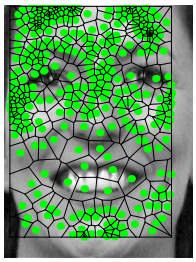

15.1: Dominant-centroids

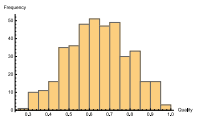

15.2: DomcentHist

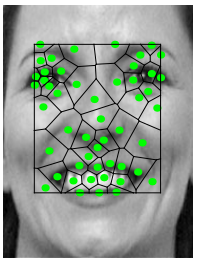

15.3: Keypoint-centroids

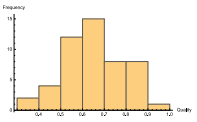

15.4: KeyptcentHist

Figure 15. Dominant & Keypoint Centroid Tessellations and Quality Histograms.

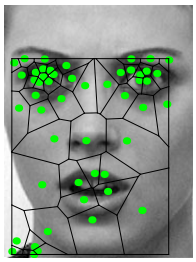

16.1: Corner-centroids

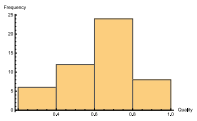

16.2: CorcentHist

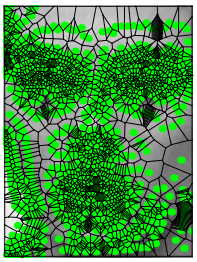

16.3: Edgecentroids

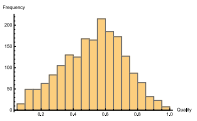

16.4: EdcentHist

Figure 16. Corner & Edge Centroid Tessellations and Quality Histograms.

Remark 6.18. Dominant centroid-Based vs.Keypoint-Based Voronoï tessellations.
Dominant generators tessellated most of the image with cells of improved qualities compared to previous situations (Fig. 19.1 and Fig. 19.2). The qualities of the cells cover the entire scale in both scenarios. However, you would notice that the cells of Fig. 19.3 are of better quality Fig. 19.4. □

Remark 6.19. Corner centroid-Based vs.Edge centroid-Based Voronoï Tessellations.
Cell qualities cover the entire scale in Fig. 20.2 and Fig. 20.4. The difference however lies in the numbers of the generators and their positions as seen in Fig. 20.1 and Fig. 20.3. □

Remark 6.20. Dominant centroid-Based vs.Keypoint-Based Voronoï tessellations.
Although common generators are returned in Fig. 21.1 and Fig. 21.3, the concentration of points in the left cheek region and the lower neck region of the test subject favored better mesh qualities generation as seen in comparing Fig. 21.2 and Fig. 21.4. □

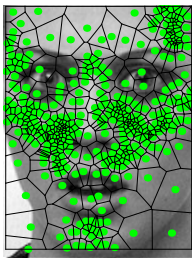

17.1: Dominant-centroids

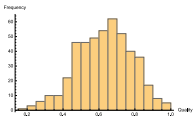

17.2: DomcenHist

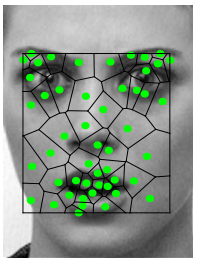

17.3: Keypoint-centroids

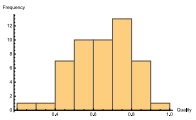

17.4: KeyptHist

Figure 17. Dominant & Keypoint Centroid Tessellations and Quality Histograms.

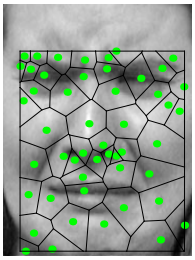

18.1: Corner-centroids

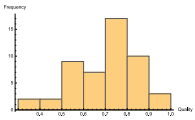

18.2: CorcentHist

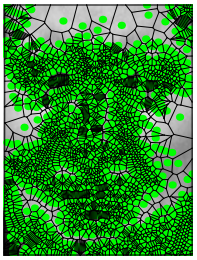

18.3: Edgecentroids

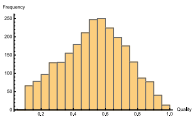

18.4: EdcentHist

Figure 18. Corner & Edge Centroid Tessellations and Quality Histograms.

The overall quality measures of meshes for each test subject class based on corner, edge, dominant and keypoint sites is presented in Fig. 22. For several images of the same subject, q_{all} is computed for each set of generators. The plot therefore presented shows the relationships of sets of generators and the overall quality of meshes for tessellated images. In the plot, the trend indicates that for sets of generators and their tessellations, keypoints give the meshes with the highest qualities. This is due to the distribution of the sites in such a way that they tend to produce perfect polygons. Edge generators on the other hand consistently give low quality tessellations. This is the case because edge sites tend to be clustered together thus producing qualities on the lower side of the scale. The qualities of corner and dominant generators assume a place in between those of edge and keypoint tessellations. The qualities of the cells by sets of generators is in proportion to distributions that tend to give perfect polygons.
The method of centroids of regions defined by image centroids shows how mesh qualities may be improved (Fig. 23). In this figure, the qualities of the cells have been improved for all sets of generators. However, the order of mesh qualities has been preserved. This improvement results from the energy minimization property of centroids and the quasi perfect polygons centroids tend to produce.

Remark 6.21. What High Quality Meshes Reveal About Tessellated Images.
Sets of sites are used to generate a Voronoï diagram (also called a mesh) on a digital image. Each

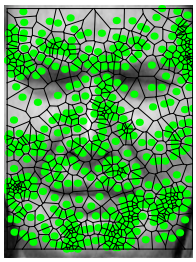

19.1: Dominant-centroids

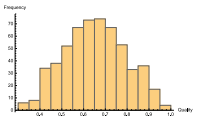

19.2: DomcentHist

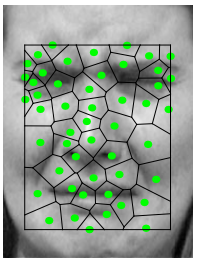

19.3: Keypoint-centroids

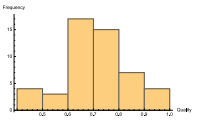

19.4: KeyptcentHist

Figure 19. Dominant & Keypoint Centroid Tessellations and Quality Histograms.

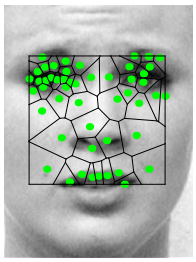

20.1: Corner-centroids

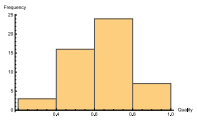

20.2: CorcentHist

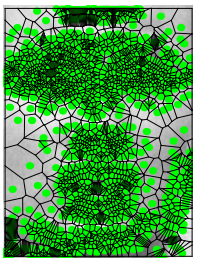

20.3: Edgecentroids

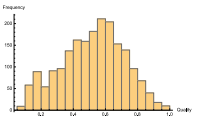

20.4: EdcentHist

Figure 20. Corner & Edge Centroid Tessellations and Quality Histograms.

region of a site is convex set represented geometrically by a polygon.

Associated with a set of sites are the qualities of the individual cells and their overall quality measure. So given sets of generators and overall tessellation qualities, the tessellation quality characterizes the underlying local structure of a collection of Voronoï regions. Quality of Voronoï polygons give us shape information about the region they cover. For the tessellated spaces, notice that the numbers of interior Voronoï polygons is greater than open border polygons. This shows that the mesh generation patterns are globular in nature. For example, the following quality expressions yielding $q = 1$ *would indicate the presence of equilateral triangle and perfect quadrilateral respectively.*

$$q = \frac{4\sqrt{3}A}{l_1^2 + l_2^2 + l_3^2}$$

$$q = \frac{4A}{l_1^2 + l_2^2 + l_3^2 + l_4^2}.$$

For small quality measurements as seen for edge point patterns sets, the measures are an indicator that the generators are on a curve and are closely spaced.

The qualities of cells and the overall quality of a tessellation characterizes the regularity and repeatability of a mesh generator set. If the space is covered with individual cells all of unit

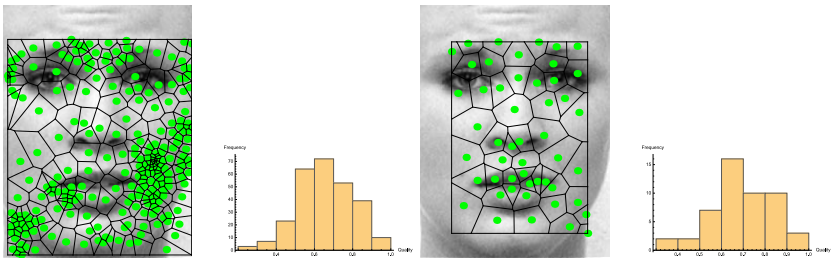

21.1: Dominant-centroids 21.2: DomcentHist 21.3: Keypoint-centroids 21.4: KeyptcentHist

Figure 21. Dominant & Keypoint Centroid Tessellations and Quality Histograms.

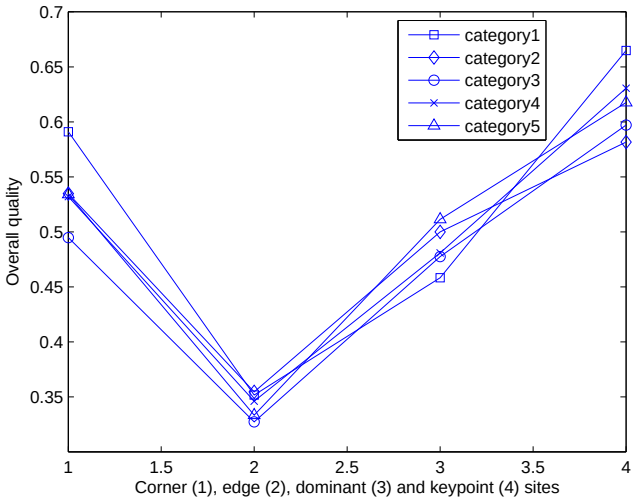

Figure 22. (a) Plot of overall quality factors against choice of sites for image categories.

quality, it indicates that the pattern points produce perfect polygons in the space. Associated with this is the simplicity of the design of the underlying pattern. Higher qualities indicate simple and predictable distributions whiles the converse holds for low qualities. This reveals the regularity of the points in the distribution of the pattern set. It also follows that the density of the points is uniform in the plane of the pattern space.

The quality of mesh cells and their associated image spaces give information on the separability of dot patterns. Generally, the higher the quality the greater the separation between points in the set. For example, the quality of edge generators is small compared to those of corners, keypoints and dominant generators and hence the separation of edge point pattern sets is poor compared to corner, keypoint and dominant pattern sets.

An extension of the separability of dot patterns and their associated factors is the notion of how adequately the point pattern represents the image space. For example if keypoints are used as mesh generators, then the generated mesh contains a distribution of polygons that surround objects in

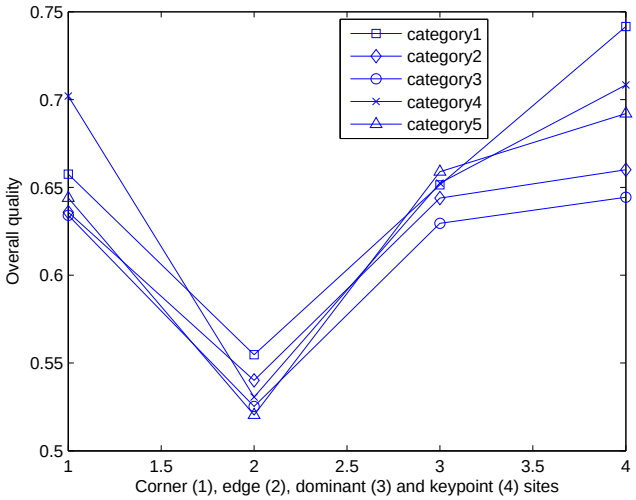

Figure 23. (a) Plot of overall quality factors against centroids of sites for image categories.

an image. In other words, the high quality of a keypoint-based mesh yields more information about image objects. To illustrate, edge tessellations give meshes with overall quality of 0.352 *versus* 0.665 *for keypoint tessellations in Fig. 24.1 and Fig. 24.2 respectively.*

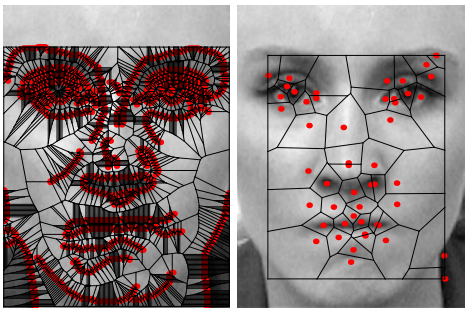

24.1: Sufficient1 24.2: Sufficient2

Figure 24. Meshes demonstrating sufficiency of coverings

Another important piece of information furnished by meshes relates to symmetry. The higher the quality, the greater the symmetry of image objects. High quality meshes tend to have connected sets of highly symmetrical polygons. To demonstrate symmetry, consider two generators $S_1(x_1, y_1)$ *and* $S_2(x_2, y_2)$ *on either side of a vertical line,* y *through a nose point. The generators* S_1 *and* S_2 *are symmetrical if and only if* $\|(x_1, y_1), y\| = \|(x_2, y_2), y\|$. *The mesh coverings in Fig. 25 are due to dominant generators and their centroids. If you draw a vertical line through the center of the nose region, you would notice that the generators in Fig. 25.2 demonstrate a better reflection of features than in Fig. 25.1. Symmetry thus furnishes us with a tool for feature location given features on one*

half of the space.

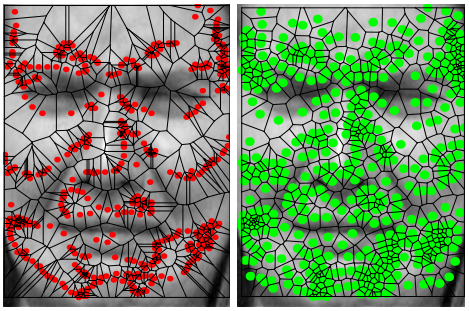

25.1: Symmetry1 25.2: symmetry2

Figure 25. Symmetry of features

Last but not least, the quality of an image mesh covering may be used to estimate image quality. Two image quality assessment methods will be compared here: Image structural similarity index (SSIM) and image quality through Voronoï tessellations. SSIM compares normalized local pixel patterns (Wang et al., 2004). For a signal pair x, y it is defined by (Wang et al., 2004)

$$SSIM(x,y) = \frac{(2\mu_x\mu_y + C_1)(2\sigma_{xy} + C_2)}{(\mu_x^2 + \mu_y^2 + C_1)(\sigma_x^2 + \sigma_y^2 + C_2)}$$

In the definition above, the SSIM between x and y uses signal statistics; the mean values of the signals μ_x, μ_y, their variances σ_x^2, σ_y^2, cross correlation between signals σ_{xy} and constants C_1 and C_2.
Voronoï mesh image quality on the other hand is defined by using the geometry of the polygons enclosing image object points and regions in a tessellated space. Given the q measures of a tessellated image space, the image quality is defined using q_{all}.
Notice that $SSIM(x,y)$ uses the entire image spaces for image quality assessment and the images must be of the same size. Besides the size constraint, huge signal sizes can make it a computationally intensive approach. Voronoï analysis of image quality on the other hand uses a small set of the features used in SSIM. To demonstrate, four image signals and their mesh coverings are given in Fig. 26 and Fig. 27 respectively.

Table 1. SSIM and Quality Indexes

Image	SSIM	q_{all}
1	0.5569	0.562207
2	-	0.581664
3	0.5969	0.538463
4	-	0.538030

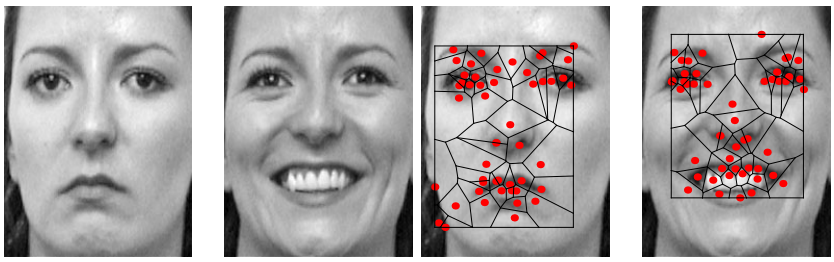

26.1: Image 1 26.2: Image 2 26.3: Meshed Covering 1 26.4: Meshed Covering 2

Figure 26. An image pair and their meshed domains for SSIM and quality comparisons

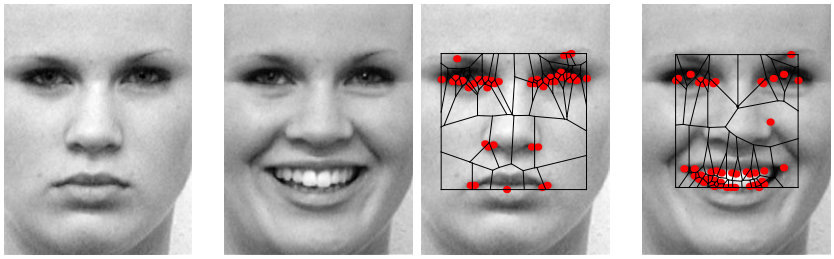

27.1: Image 3 27.2: Image 4 27.3: Meshed Covering 3 27.4: Meshed Covering 4

Figure 27. An image pair and their meshed domains for SSIM and quality comparisons

Image quality indicators of the signals in Fig. 26 and Fig. 27 is reported in Table. 1. Note that although the entire feature space is utilized in the calculation of the SSIM, they are comparable with those obtained with Voronoï tessellations. Notwithstanding, the Voronoï image quality method provides a quality indicator for each image whereas two signals are needed to output their SSIM. The ideal index possible is 1. *An image Voronoï index of 1 means that the point pattern spatial geometry or arrangement is perfectly regular while an SSIM of 1 would mean a perfect match between the two images.*

□

Note that there are differences between the SSIM and q_{all} indexes, although small. The differences stem from the fact that the mesh approach uses polygonal regions and their shape information to capture image quality, whilst the SSIM index depends on all pixel values in the image. Also, the SSIM index depends on constants, as it it affects the indicators. The mesh approach however depends on image features only.

Note that mesh qualities show that low overall quality generators are not sufficient descriptors of image features. On the other hand high mesh qualities indicate important and influential image

features useful for image and mesh analysis. Also, note that the numbers of generator sites are different for corner, edge, dominant and keypoint sites. Even though edges tend to have the highest numbers, their qualities are very poor in comparison to the other generators. This shows that high quality meshes such as those generated by keypoints identify better the most influential, more well laid out and important features in image characterization and representation.

7. Conclusion

Voronoï generating points useful in image tessellations and visual image quality analysis have been identified. Previous works focused on generating points based on random distributions, sites without consideration of feature locations with scant attention given to resulting mesh quality. Various mathematical results pertaining to meshes, quality have been identified and proved. Centroidal tessellations have been used as a means to improve tessellation quality. This appears to be a new way of tessellation quality improvement as the literature hardly considers feature-based centroidal tessellations and resulting qualities. The measurement of image mesh quality offers a means of choosing suitable mesh generating points or sites based on their sufficiency in characterizing features of digital images. An important limitation of the model here is that slight perturbation of generators would mean changing locations leading to possibly different polygonal lengths and areas, hence the need to readjust or compute quality measures. Choosing a subset of the entire signal space for generators does not seem to be a significant limitation since it usually covers a significant portion of the space. However, we can always increase the numbers of generators to cover larger spaces although at higher computational costs.

References

Agrell, Erik (1996). Voronoi regions for binary linear block codes. *Information Theory, IEEE Transactions on* **42**(1), 310–316.

Ahuja, Narendra and Bruce Jay Schachter (1982). *Pattern models*. John Wiley & Sons Inc.

Arbeláez, Pablo A and Laurent D Cohen (2006). A metric approach to vector-valued image segmentation. *International Journal of Computer Vision* **69**(1), 119–126.

Aurenhammer, Franz (1991). Voronoi diagrams - a survey of a fundamental geometric data structure. *ACM Computing Surveys (CSUR)* **23**(3), 345–405.

Bank, R.E. and J. Xu (1996). An algorithm for coarsening unstructured meshes. *Numerische Mathematik* **73**, 1–36.

Bern, Marshall and P Plassmann (1999). Mesh generation. *Handbook of Computational Geometry*.

Bhatia, RP and KL Lawrence (1990*a*). Two-dimensional finite element mesh generation based on stripwise automatic triangulation. *Computers & Structures* **36**(2), 309–319.

Bhatia, R.P. and K.L. Lawrence (1990*b*). Two-dimensional finite element mesh generation based on stripwise automatic triangulation. *Computers & Structures* **36**(2), 309–319.

Brauwerman, Roger, Sarah Joy Zoll, Christopher L Farmer and Max Gunzburger (1999). Centroidal voronoi tessellations are not good jigsaw puzzles. http://www.math.iastate.edu/reu/1999/cvt.pdf.

Brown, Matthew and David G Lowe (2002). Invariant features from interest point groups.. In: *BMVC*. number s 1.

Burns, Jared (2009). Centroidal voronoi tessellations. https://www.whitman.edu/Documents/Academics /Mathematics/burns.pdf.

Canny, John (1986). A computational approach to edge detection. *Pattern Analysis and Machine Intelligence, IEEE Transactions on* (6), 679–698.

Craw, Ian (2009). 2d face sets. http://pics.stir.ac.uk/2D_face_sets.htm. Pain Expression Subset.

Demir, Cigdem and Bülent Yener (2005). Automated cancer diagnosis based on histopathological images: a systematic survey. *Rensselaer Polytechnic Institute, Tech. Rep*.

Du, Qiang, Vance Faber and Max Gunzburger (1999). Centroidal voronoi tessellations: applications and algorithms. *SIAM review* **41**(4), 637–676.

Ebeida, Mohamed S and Scott A Mitchell (2012). Uniform random voronoi meshes. In: *Proceedings of the 20th International Meshing Roundtable*. pp. 273–290. Springer.

Ebeida, Mohamed S, Scott A Mitchell, Andrew A Davidson, Anjul Patney, Patrick M Knupp and John D Owens (2011). Efficient and good delaunay meshes from random points. *Computer-Aided Design* **43**(11), 1506–1515.

Feng, Xiaoyi, Yangming Lai, Xiaofei Mao, Jinye Peng, Xiaoyue Jiang and Abdenour Hadid (2013). Extracting local binary patterns from image key points: Application to automatic facial expression recognition. In: *Image Analysis*. pp. 339–348. Springer.

Field, D.A. (2000). Qualitative measures for initial meshes. *Int. J. for Numerical Methods in Engineering* **47**, 887–906.

Förstner, Wolfgang and Eberhard Gülch (1987). A fast operator for detection and precise location of distinct points, corners and centres of circular features. In: *Proc. ISPRS intercommission conference on fast processing of photogrammetric data*. pp. 281–305.

George, Paul Louis (2006). Adaptive mesh generation in 3 dimensions by means of a delaunay based method. applications to mechanical problems. In: *III European Conference on Computational Mechanics*. Springer. pp. 18–18.

Guru, DS and R Dinesh (2004). Non-parametric adaptive region of support useful for corner detection: a novel approach. *Pattern Recognition* **37**(1), 165–168.

Hamanaka, Masatoshi and Keiji Hirata (2002). Applying voronoi diagrams in the automatic grouping of polyphony. *Information Technology Letters* **1**(1), 101–102.

Harris, Chris and Mike Stephens (1988). A combined corner and edge detector.. In: *Alvey vision conference*. Vol. 15. Manchester, UK. p. 50.

Kang, Sung Kwan, Young Chul Choung and Jong An Park (2005). Image corner detection using hough transform. In: *Pattern Recognition and Image Analysis*. pp. 279–286. Springer.

Kim, Bongjoe, Jihoon Choi, Yongwoon Park and Kwanghoon Sohn (2012). Robust corner detection based on image structure. *Circuits, Systems, and Signal Processing* **31**(4), 1443–1457.

Kitchen, Les and Azriel Rosenfeld (1980). Gray-level corner detection. Technical report. DTIC Document.

Knupp, Patrick M (2001). Algebraic mesh quality metrics. *SIAM journal on scientific computing* **23**(1), 193–218.

Koenderink, Jan J and Whitman Richards (1988). Two-dimensional curvature operators. *JOSA A* **5**(7), 1136–1141.

Leibon, Greg and David Letscher (2000). Delaunay triangulations and voronoi diagrams for riemannian manifolds. In: *Proceedings of the sixteenth annual symposium on Computational geometry*. ACM. pp. 341–349.

Lindeberg, Tony (1993). *Scale-space theory in computer vision*. Springer Science & Business Media.

Lindeberg, Tony (1998). Feature detection with automatic scale selection. *International journal of computer vision* **30**(2), 79–116.

Lindeberg, Tony (2008). *Scale-Space*. Wiley Online Library.

Liu, Jinyi and Shuang Liu (2004). A survey on applications of voronoi diagrams. *Journal of Engineering Graphics* **22**(2), 125–132.

Lowe, David G (1999). Object recognition from local scale-invariant features. In: *Computer vision, 1999. The proceedings of the seventh IEEE international conference on*. Vol. 2. Ieee. pp. 1150–1157.

Lowe, David G (2004). Distinctive image features from scale-invariant keypoints. *International journal of computer vision* **60**(2), 91–110.

McLean, Alex (2007). Voronoi diagrams of music. *URL http://doc. gold. ac. uk/˜ ma503am/essays/voronoi/voronoi-diagrams-of-music. pdf. Accessed*.

Mikolajczyk, Krystian and Cordelia Schmid (2004). Scale & affine invariant interest point detectors. *International journal of computer vision* **60**(1), 63–86.

Mitchell, HB (2010). Image key points. In: *Image Fusion*. pp. 163–166. Springer.

Mitchell, Scott A (1993). Mesh generation with provable quality bounds. Technical report. Cornell University.

Møller, Jesper and Øivind Skare (2001). Coloured voronoi tessellations for bayesian image analysis and reservoir modelling. *Statistical modelling* **1**(3), 213–232.

Moravec, Hans P (1980). Obstacle avoidance and navigation in the real world by a seeing robot rover.. Technical report. DTIC Document.

Owen, Steven J (1998). A survey of unstructured mesh generation technology. In: *IMR*. pp. 239–267.

Pan, Haixia, Yanxiang Zhang, Chunlong Li and Huafeng Wang (2014). An adaptive harris corner detection algorithm for image mosaic. In: *Pattern Recognition*. pp. 53–62. Springer.

Park, Seung Jin, Muhammad Bilal Ahmad, Rhee Seung-Hak, Seung Jo Han and Jong An Park (2004). Image corner detection using radon transform. In: *Computational Science and Its Applications–ICCSA 2004*. pp. 948–955. Springer.

Peraire, Jaime, Morgan Vahdati, Ken Morgan and Olgierd C Zienkiewicz (1987). Adaptive remeshing for compressible flow computations. *Journal of computational physics* **72**(2), 449–466.

Persson, Per-Olof (2004). Mesh generation for implicit geometries. PhD thesis. Citeseer.

Persson, Per-Olof and Gilbert Strang (2004). A simple mesh generator in matlab. *SIAM review* **46**(2), 329–345.

Peters, J.F. (2015*a*). Proximal Delaunay triangulation regions. *PJMS [Proc. Jangjeon Math. Soc.]* pp. 1–10. *accepted*.

Peters, J.F. (2015*b*). Proximal Voronoï regions, convex polygons, & Leader uniform topology. *Advances in Math.: Sci. J.* **4**(1), 1–5.

Peters, J.F. (2015*c*). Visibility in proximal Delaunay meshes and strongly near Wallman proximity. *Advances in Math.: Sci. J.* **4**(1), 41–47.

Rajan, V.T. (1994). Optimality of the delaunay triangulation in $\mathbb{R}^d$. *Discrete & Computational Geometry* **12**(1), 189 – 202.

Ramella, Massimo, Mario Nonino, Walter Boschin and Dario Fadda (1998). Cluster identification via voronoi tessellation. *arXiv preprint astro-ph/9810124*.

Rivara, Maria-Cecilia (1984). Mesh refinement processes based on the generalized bisection of simplices. *SIAM Journal on Numerical Analysis* **21**(3), 604–613.

Rosten, Edward and Tom Drummond (2006). Machine learning for high-speed corner detection. In: *Computer Vision–ECCV 2006*. pp. 430–443. Springer.

Ruppert, Jim (1995). A delaunay refinement algorithm for quality 2-dimensional mesh generation. *Journal of algorithms* **18**(3), 548–585.

Shewchuk, J (2002). What is a good linear finite element? interpolation, conditioning, anisotropy, and quality measures (preprint). *University of California at Berkeley*.

Smith, Stephen M. and J. Michael Brady (1997). SUSAN - a new approach to low level image processing. *International journal of computer vision* **23**(1), 45–78.

Voronoï, G. (1903). Sur un problème du calcul des fonctions asymptotiques. *J. für die reine und angewandte Math.* **126**, 241–282. JFM 38.0261.01.

Voronoï, G. (1907). Nouvelles applications des paramètres continus à la théorie des formes quadratiques. premier mémoir. *J. für die reine und angewandte Math.* **133**, 97–178.

Voronoï, G. (1908). Sur un problème du calcul des fonctions asymptotiques. *J. für die reine und angewandte Math.* **134**, 198–287. JFM 39.0274.01.

Wang, Han and Michael Brady (1995). Real-time corner detection algorithm for motion estimation. *Image and Vision Computing* **13**(9), 695–703.

Wang, Zhou, Alan C Bovik, Hamid R Sheikh and Eero P Simoncelli (2004). Image quality assessment: From error visibility to structural similarity. *Image Processing, IEEE Transactions on* **13**(4), 600–612.

Woźniak, Marcin and Zbigniew Marszałek (2014). An idea to apply firefly algorithm in 2d image key-points search. In: *Information and Software Technologies*. pp. 312–323. Springer.